Power Electronic Systems
Laboratory

IEEE Transactions on Power Electronics, Vol. 29, No. 8, pp. 4078-4090, August 2014

Flux Balancing of Isolation Transformers and Application of „the Magnetic Ear“ for Closed-Loop Volt-Second Compensation

G. Ortiz,
L. Fässler,
J. W. Kolar,
O. Apeldoorn

Eidgenössische Technische Hochschule Zürich
Swiss Federal Institute of Technology Zurich

Flux Balancing of Isolation Transformers and Application of "The Magnetic Ear" for Closed-Loop Volt–Second Compensation

Gabriel Ortiz, *Member, IEEE*, Lukas Fässler, Johann Walter Kolar, *Fellow, IEEE*, and Oscar Apeldoorn

***Abstract*—Semiconductor switches possess nonideal behavior which, in case of isolated dc–dc converters, can generate dc-voltage components which are then applied to the isolation transformer. This dc-voltage component is translated into a dc flux density component in the transformer core, increasing the risk of driving the core into saturation. In this paper, a novel noninvasive flux density measurement principle, called "The Magnetic Ear," based on sharing of magnetic path between the main and an auxiliary core is proposed. The active compensation of the transformer's dc magnetization level using this transducer is experimentally verified. Additionally, a classification of the previously reported magnetic flux measurement and balancing concepts is performed.**

***Index Terms*—Magnetic analysis, magnetic cores, magnetic transducers, magnetic variables measurement, measurement, transducers.**

I. Introduction

ISOLATED and/or high step-up dc–dc converters are built with arrangements of semiconductor switches which provide ac excitation to a transformer. Phenomena such as unmatched turn-on/turn-off times, semiconductor forward voltage drop, gate driving signal delays, insufficient pulse width modulation (PWM) resolution, or pulsating load, among others, can cause differences in the positive and negative volts–seconds applied to the transformer [1]. This results in a dc-voltage component at the transformer terminals, which causes an undesired dc magnetic flux density component in the transformer core.

In order to show the relation between this voltage and magnetic flux density dc components, consider the circuit presented in Fig. 1(b), where a dual active bridge (DAB) dc–dc converter topology is shown. The primary and secondary bridges apply voltages $v_{\rm p}(t)$ and $v_{\rm s}(t)$ to the transformer, respectively. The dc and the ac components of these voltages can be separated into independent voltage sources, building the circuit depicted in Fig. 1(c), where the secondary side has been reflected to the primary side. Here, the resistances $R_{\rm p,T}$ and $R'_{\rm s,T}$ represent the winding resistances $R_{\rm p,s}$ and $R'_{\rm s,s}$ plus the semiconductors' equivalent on-state resistances of the primary and secondary side switches, respectively.

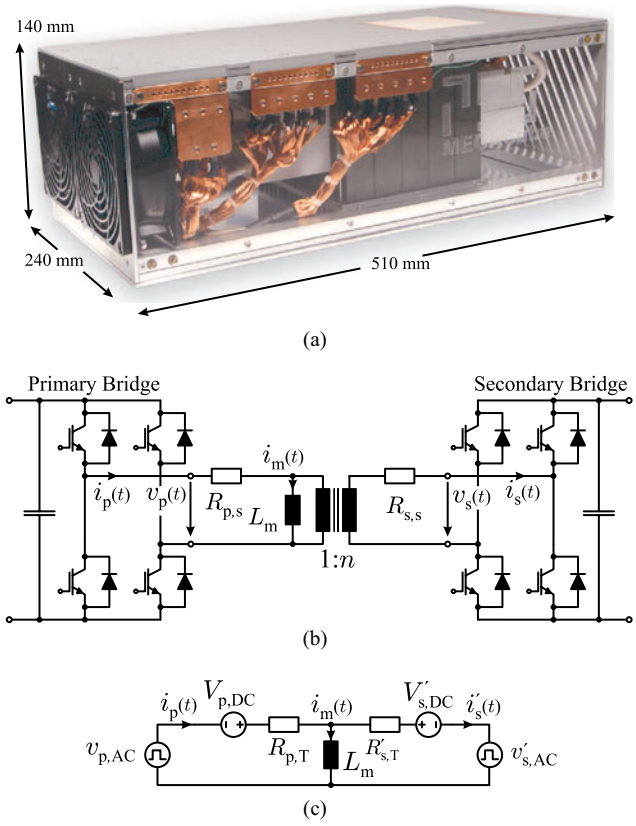

Fig. 1. (a) MEGACube transformer [2], [3] optimized for efficiency. (b) DAB converter with simplified transformer model. (c) Equivalent model of the converter with independent dc and ac voltage sources and reflected secondary side.

In steady state, the dc part of the magnetizing current $I_{\rm m,dc}$ of the transformer is given by

$$I_{\rm m,dc} = I_{\rm p,dc} - I'_{\rm s,dc} = \frac{V_{\rm p,dc}}{R_{\rm p,T}} - \frac{V'_{\rm s,dc}}{R'_{\rm s,T}}\,. \tag{1}$$

The dc magnetic flux density is then determined by the characteristics of the winding and core through

$$B_{\rm dc} = \frac{I_{\rm m,dc}\cdot N_{\rm p}}{l_{\rm m}}\cdot\mu_0\bar{\mu}_{\rm r} = \left(\frac{V_{\rm p,dc}}{R_{\rm p,T}} - \frac{V'_{\rm s,dc}}{R'_{\rm s,T}}\right)\cdot\frac{N_{\rm p}}{l_{\rm m}}\cdot\mu_0\bar{\mu}_{\rm r} \tag{2}$$

Manuscript received July 18, 2013; revised November 14, 2013; accepted November 25, 2013. Date of current version March 26, 2014. Recommended for publication by Associate Editor S. K. Mazumder.

G. Ortiz, L. Fässler, and J. W. Kolar are with the Power Electronic Systems Laboratory, ETH Zurich, 8092 Zurich, Switzerland (e-mail: ortiz@lem.ee.ethz.ch; faessler@lem.ee.ethz.ch; kolar@lem.ee.ethz.ch).

O. Apeldoorn is with the Power Electronics and Medium Voltage Drives, ABB Switzerland Ltd., CH-5300 Turgi, Switzerland (e-mail: oscar.apeldoorn@ch.abb.com).

Color versions of one or more of the figures in this paper are available online at http://ieeexplore.ieee.org.

Digital Object Identifier 10.1109/TPEL.2013.2294551

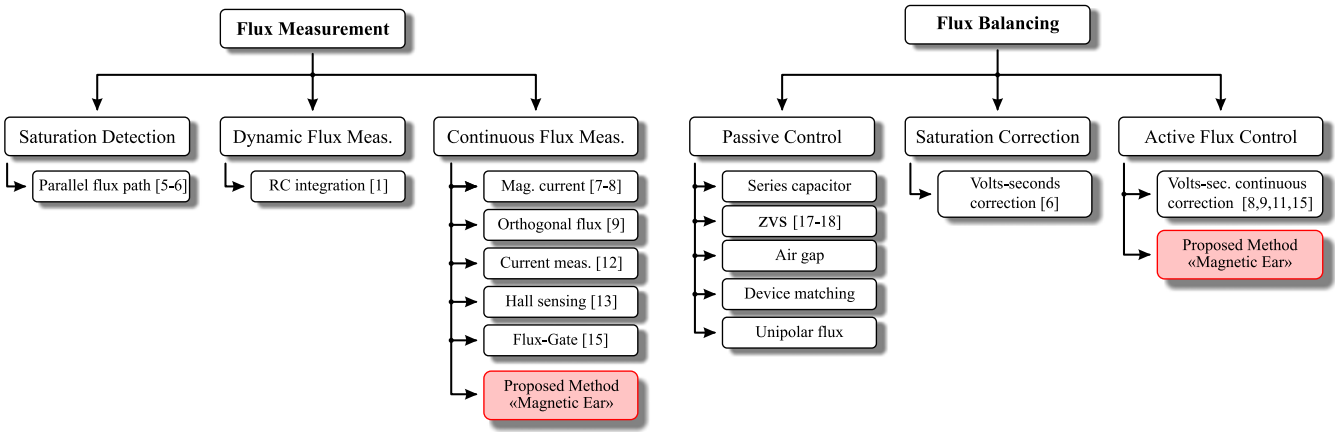

Fig. 2. Classification of previously proposed flux balancing concepts. The two main areas are flux measurement and flux feedback control. The proposed measurement concept, "The Magnetic Ear," is highlighted within this classification.

where l_{m} is the length of the magnetic path, N_{p} is the number of turns in the primary side, μ_0 is the permeability of air, and $\bar{\mu}_{\mathrm{r}}$ is the core's relative permeability in the linear region of the B–H curve.

From (2), it can be seen that the dc magnetic flux density is limited by the equivalent series resistances, $R_{\mathrm{p,T}}$ and $R'_{\mathrm{s,T}}$, of the circuit, which are typically kept as low as possible in order to decrease the converter's conduction losses. This means that a small dc component in the voltage applied to the transformer generates a large dc flux density component.

For example, taking the shell-type 166-kW/20-kHz efficiency-optimized transformer [3] [cf. Fig. 1(a)] with suitable switches on the primary side, the primary side equivalent resistance $R_{\mathrm{p,T}}$ reaches 1.7 mΩ. This design considers a Ferrite N87 core material which is characterized by a relative permeability $\bar{\mu}_{\mathrm{r}}$ around 1950. In this design, a 0.0125% of relative difference in the duration of the positive and negative semicycles of the primary voltage $v_{\mathrm{s}}(t)$, i.e., a switching time error of 2.5 ns, would suffice to create a dc flux density component of $B_{\mathrm{dc}} = 50$ mT.

With this dc flux density component, the core can be easily driven outside the linear region of the B–H curve, generating a nonlinear magnetizing current with high peak values. This results in increased conduction and switching losses, causing reduction in efficiency and higher semiconductor and transformer operating temperatures, compromising the converter's reliability. Moreover, a dc-biased flux density waveform results in higher core losses [4], further compromising the converter's efficiency. For these reasons, the operation of the transformer under balanced condition, i.e. with zero dc flux density component, must be ensured. It is also worth to note that if a balanced operation of the flux density in the core is ensured, the transformer can be designed with low flux density overdimensioning, meaning that its magnetic cross section, and therefore its volume, can be reduced, increasing the converter's power density.

In order to ensure balanced flux operation, the main problems that must be addressed are measurement of the core's internal flux status (see Section I-A) and balancing or closed-loop control of the flux (see Section I-B). Within these two topics, other

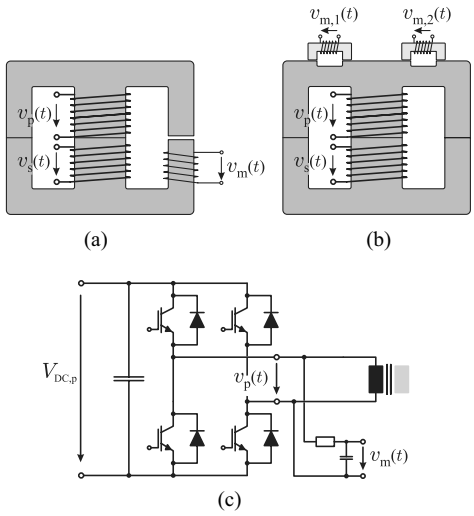

Fig. 3. Previously proposed concepts for magnetic saturation prevention: (a) Parallel magnetic path in an E-core with a gaped leg [5]. (b) Parallel magnetic path with external cores and reduced cross section [6]. (c) Integration of applied voltage with an *RC* network [7].

subcategorizations are possible, as displayed in Fig. 2 and discussed in the following sections.

A. Flux Measurement/Saturation Detection

The methods for recognition of the core's flux state can be classified into: *1) saturation detection*; *2) dynamic flux measurement,*; and *3) continuous flux behavior measurement*. The measurement method proposed in this paper lies in this last class.

1) Saturation Detection: In [5], an E-core was used with an air-gap in one of the external legs [see Fig. 3(a)]. During the normal operation, the flux flows only in the ungapped leg but as soon as this leg saturates, part of magnetic flux is forced through the gapped leg, and therefore, a voltage can be induced in an additional winding, detecting the saturation of the main flux path. Alternatively, in [6], a slot is placed in one of the core legs, as shown in Fig. 3(b) in order to reduce the cross-sectional

area in this place. An additional magnetic path with a winding is provided parallel to the slotted part of the core. As the slotted section has a smaller area, it saturates at lower flux densities with respect to the rest of the core, and therefore, the magnetic flux is forced into this parallel magnetic path. This induces a voltage in a winding indicating the impending core saturation.

With both these methods, only the saturation of the core is detected, which may be enough in some applications. In applications which require high efficiency, however, this is not enough since the flux density in the core can still be biased without being saturated, and therefore, the core losses are increased. Moreover, in order to implement both these methods, modifications to the magnetic components are required, increasing its cost and complexity.

2) Dynamic Flux Measurement: This method was proposed in [7] in order to detect flux unbalance due to variations in the converter loading conditions. The principle is to perform an integration of the applied voltage through an *RC* network or an active integrator [cf., Fig. 3(c)]. This integrated signal is proportional to the core's magnetic flux. Due to the requirement of an integration, this method can only sense dynamic variations of the flux, i.e., steady-state asymmetries will not be detected.

3) Continuous Flux Behavior Measurement: The sensing of the flux behavior with large bandwidth and independent of the operating conditions has been covered by several publications, where the following main categories can be identified:

a) Magnetizing Current Measurement: The magnetizing current $i_{\mathrm{m}}(t)$ indicates the status of flux density in the core. The measurement of this current through subtraction of the scaled primary and secondary currents was proposed in [7].

In [8], and later in [10], a measurement of the magnetizing current was performed by building an additional transformer with the same turns ratio as the main transformer but with one of the windings in the inverted orientation [cf., Fig. 4(a)]. This transducer effectively operates as a mutual magnetic compensator similar to other current sensing concepts, and is therefore able to sense dc components on the transformer's magnetic flux density.

The disadvantage of this method is the requirement of isolation on the additional transformer, which needs to be at least the same as the one of the main core. Also, practical issues may arise in higher power transformers where the wiring of primary and secondary sides has an increased complexity [3].

b) Orthogonal Magnetic Fluxes: In [9], the internal core flux was measured by using an additional coil fed by a dc current which generates a magnetic flux orthogonal to the main flux [cf., Fig. 4(c)]. The orthogonality of the magnetic fluxes ensures that no voltage is induced in the additional coil due to the main flux. As the main magnetic flux density is changed, the B–H characteristic of the material is also changing. This material property change is translated into a variation of the flux in the orthogonal coil, inducing a voltage in its terminals. This principle was also proposed for microfabricated inductors [11] in order to intentionally shape the B–H loop of the magnetic material. In this concept, modified or specially shaped cores are required in order to insert the orthogonal winding, increasing its cost and complexity. Moreover, if the B–H loop has a large linear region, voltage would be induced in the orthogonal coil only when the core is saturated.

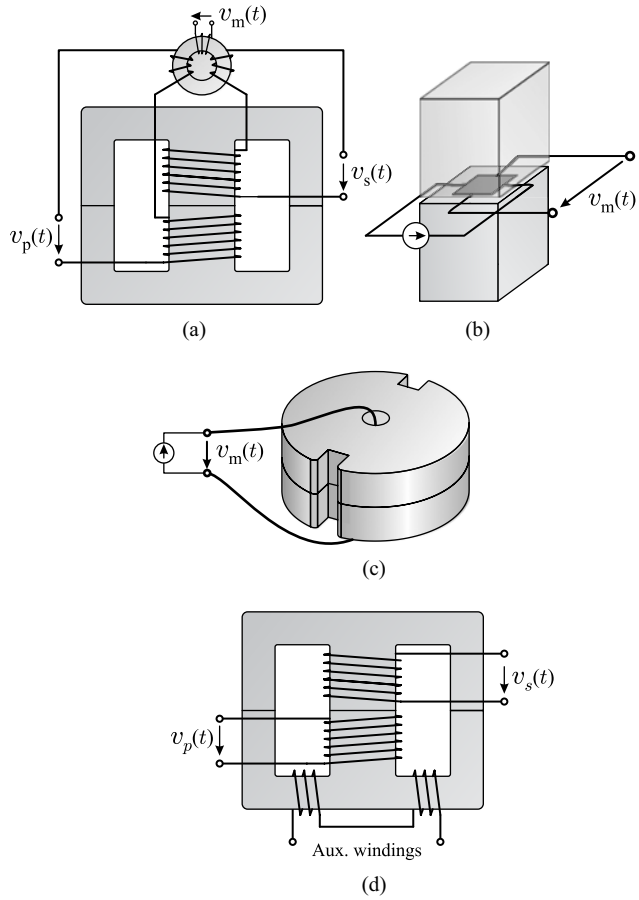

Fig. 4. Continuous measurement of core's internal flux: (a) Construction of the magnetizing current with an external transformer [8]. (b) Magnetic flux measurement with the Hall sensor in magnetic path. (c) Orthogonal magnetic fluxes [9].

c) Converter Current Measurement and Processing: The direct measurement of the primary and/or the secondary currents has also been used to balance the flux in the core. As an example, the dc magnetization of the core generates primary/secondary currents with even numbered Fourier components. The amplitude of these components can be measured and used as feedback signal to balance the transformer flux, as was performed in [12].

In converters with modulations which do not operate always at 50% duty cycle, only the magnetizing current is present during the freewheeling periods. This current can be measured during these intervals obtaining information about the status of the core's flux. In this case, however, high vertical resolution is required on the analog-to-digital converter since typically at these power levels, the magnetizing current is very low compared to the main current; thus, its detection becomes a major challenge.

d) Flux Observer: In order to overcome the limitation of only dynamic flux measurement, the method described in Section I-A2 can be complemented with a measurement of the transformer current [7]. This way, an observer that reconstructs the flux density based would be feasible.

e) Hall Sensing: The most direct way to measure the flux in the core would be to insert a thin hall sensor in the magnetic flux path [13] [cf., Fig. 4(b)]. However, this requires the insertion of an air gap in the magnetic core, reducing the magnetizing inductance and increasing the reactive power provided to the transformer. Moreover, the fabrication of the Hall sensor presents major challenges, as known from current sensor manufacturing.

f) Flux-Gate: The flux-gate principle is a well-known concept for current measurement [14]. This measurement principle can be adapted in order to build a flux-density transducer, as presented in [15] and shown in Fig. 4(d). In this concept, an E-type core is utilized whereby the primary and secondary windings are placed around the core's middle leg while two additional windings are placed in one of the "I" parts of the core, as depicted in Fig. 4(d). With this arrangement, a dc bias in the flux-density would result in a change in the inductance in the terminals of the auxiliary winding, thus enabling monitoring of the flux density in the core.

The main disadvantage of this concept is the requirement of full isolation between the auxiliary windings and the primary and secondary windings. Additionally, the auxiliary windings must be placed in the core window, therefore reducing the respective filling factor.

B. Flux Balancing/Feedback Control

The internal core flux can be passively or actively balanced. Depending on whether the measuring principle detects core saturation or performs a complete flux measurement, the active flux balancing principles can be subdivided into saturation correction or continuous flux control.

1) Passive Balancing: Passive balancing refers to any balancing principle which does not actively modify the switching signals of the semiconductor devices in order to keep the transformer flux between safe margins. The following passive flux balancing principles can be pointed out:

a) Series Capacitor: One of the most utilized flux balancing principles, due to its simplicity, is the inclusion of a capacitor in series to the transformer winding. The main disadvantages of this approach are 1) increased converter volume, 2) increased converter losses, and 3) slow dynamic response. This idea was further developed in [16] where a resistor was placed in parallel to the capacitor in order to improve low-frequency behavior.

b) Zero-Voltage-Switching: Ensuring zero-voltage-switching (ZVS) of all converter semiconductor devices partially compensates for mismatches in the volts–seconds applied to the transformer, as presented in [17] and [18]. Here, the modification of the current shape due to the biased operation results in an inherent modification of the voltage waveform during the switching intervals, therefore positively affecting the volts–seconds applied to the transformer which partially compensates for the biased operation.

c) Air-gap in Core's Magnetic Path: When an air-gap is included in the core's magnetic path, the permeability of the core is effectively decreased. This in turn increases the tolerable dc magnetization but does not eliminate the dc flux component as with a series capacitor; thus, this is not strictly a flux balancing method. Moreover, the inclusion of an air-gap in the core decreases the value of magnetizing inductance L_{m}, increasing the switched and conducted currents.

In addition to the previously presented passive flux balancing principles, the prevention of core saturation can be included as part of the converter design process. In [1], the different converter electrical parameters that influence the core saturation were clearly pointed out and used to give design considerations which help avoiding it.

2) Active Saturation Correction: The flux measuring concepts presented in Section I-A1 can be used in order to implement feedback control which only operates under impending core saturation, as was done in [5].

3) Active Feedback Control of the Flux: If a signal proportional to the internal core flux density is available, the dc magnetization of the core can be actively controlled by modifying the volts–seconds applied to the transformer. The main feedback flux control principles that have been proposed are detailed in [7]–[9], [13], and [19]. The feedback scheme proposed in this paper is revised in Section IV.

In this paper, a novel magnetic flux density transducer is introduced and its operating principle is experimentally verified. The measured transducer signal is used to perform a closed-loop flux balancing control, ensuring the operation of the transformer core within safe flux density values. The proposed flux density transducer is described in Section II and the design tradeoffs regarding this transducer are presented in Section III. In Section IV, the output signal of the transducer is used in order to perform a closed-loop compensation of the flux density in the transformer core.

II. The Magnetic Ear

The main requirements for a flux density transducer in MF high-power applications can be summarized as follows:

1) *Continuous monitoring:* Since the MF transformer is a critical component within high-power dc–dc converters, it is desirable to continuously monitor the magnetization state of the transformer core.
2) *Isolation:* The measurement concept needs to be specified for the same isolation level as the main transformer.
3) *Noninvasive:* Due to the high complexity and cost of MF transformer technologies, it is highly desirable to realize the design of this component independent from its magnetic flux-density measurement concept, i.e., a flux measurement principle which does not interfere with the MF transformer design is required.

Accordingly, a novel magnetic flux density transducer, The Magnetic Ear, which complies with these requirements is proposed and extensively studied in the following. The Magnetic Ear's main concept consists of a shared magnetic path between the main core (the actual transformer core) and an auxiliary core represented by the reluctance R_{m} in Fig. 5(a), where the transformer serves as link between the primary and secondary side full-bridges, building a DAB configuration as already discussed in Fig. 1(b). This shared reluctance R_{m} changes its magnetic

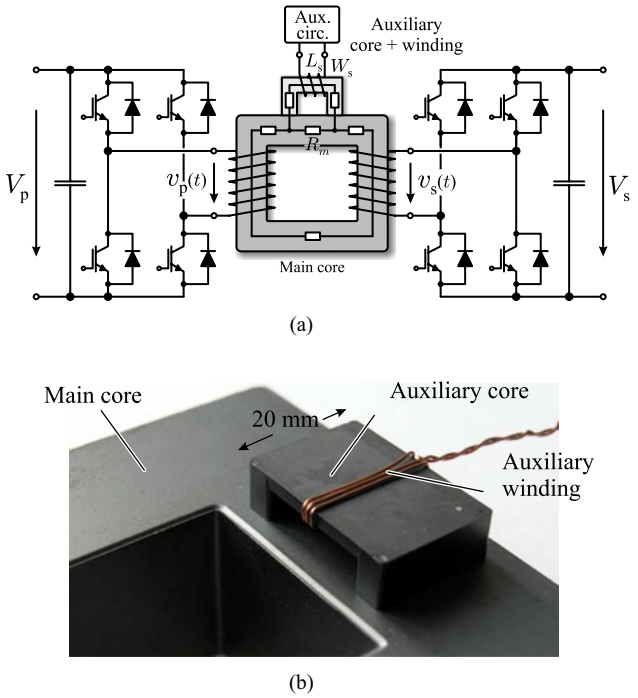

Fig. 5. The Magnetic Ear main concept: (a) Equivalent circuit representation with main core and auxiliary core sharing part of the magnetic path. (b) Real implementation of the main core (EPCOS UU93/76/30 N87) and auxiliary core (EPCOS EQ30/8 N87 with removed middle leg) and $N_{\mathrm{aux}} = 3$.

properties, namely its relative permeability $\mu_{\mathrm{r,m}}$ as the main core is driven through the B–H loop. This variation results in a change in the inductance L_{s} measured from the terminals of the auxiliary core's winding W_{s}. This variation in the inductance is sensed by an auxiliary drive circuit which extracts the inductance value of the auxiliary core, delivering a signal directly related to the instantaneous magnetization state of the core. The main and auxiliary cores used to test this concept are presented in Fig. 5(b).

The B–H loop of the transformer in Fig. 1(a) is presented in Fig. 6(a), while the measurement of the inductance for the auxiliary core arrangement shown in Fig. 5(b) is presented in Fig. 6(b), whereby the main and auxiliary cores are built with EPCOS UU93/76/30 N87 and EPCOS EQ30/8 N87 cores, respectively. As can be seen, the inductance of the auxiliary core is considerably sensible to the instantaneous magnetization state of the main core; thus, the instantaneous value of the auxiliary core's inductance can be used as measure of the magnetization state of the main core. It should be noted that the behavior of the auxiliary core's inductance is depending on the shape of the main core's B–H loop, whereby higher sensitivities are reached if the permeability of the main core continuously changes along the B–H loop. In case, the core material is highly linear until saturation is reached, e.g., in gapped cores, this sensitivity is deteriorated and only a change in the inductance can be perceived once the core is driven into saturation. The details and tradeoffs in the transducer's design, which is ultimately used to control the flux in the main core, will be discussed in the following.

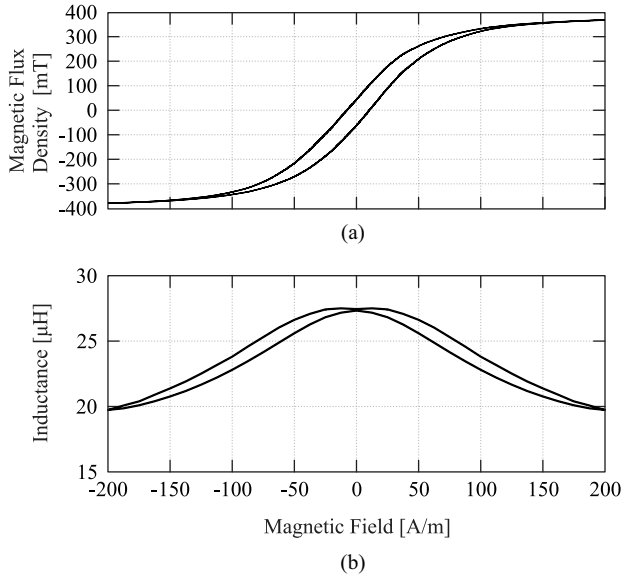

Fig. 6. (a) B–H loop of the transformer core shown in Fig. 1. (b) Measured inductance from the auxiliary core's terminals as the main core is driven through the B–H loop.

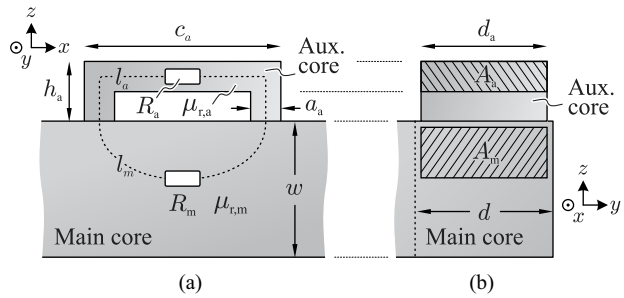

Fig. 7. Magnetic flux density transducer, The Magnetic Ear, geometric definitions.

III. Design, Drive Circuits, and Sampling Methods

As mentioned earlier, The Magnetic Ear transducer consists of an auxiliary core with its auxiliary winding and the respective drive circuit used to measure the inductance seen from the auxiliary winding terminals and to convert it to an analog signal. Moreover, in order to implement the feedback loop which performs the flux balancing in the main transformer core, the sampling strategy of the aforementioned signal needs to be studied. As a start, the selection of the appropriate auxiliary core geometry (dimensions) and core material is addressed.

A. Auxiliary Core Design

The selection of the auxiliary core's shape and magnetic properties, namely its relative permeability $\mu_{\mathrm{r,a}}$, will directly affect the sensitivity of the auxiliary inductance L_{aux} to changes in the main core's permeability $\mu_{\mathrm{r,m}}$, i.e., changes in the magnetization state of the main core.

In order to analyze the impact of the auxiliary core's geometry and its magnetic properties on the measurement sensitivity, consider the arrangement presented in Fig. 7(a), where a C core is used as auxiliary core. In order to achieve a high

sensitivity to changes in the main core's permeability $\mu_{\mathrm{r,m}}$, the total reluctance of the auxiliary core's magnetic path must be mainly defined by the shared reluctance R_{m} and not by the auxiliary core's reluctance R_{a}, i.e., $R_{\mathrm{m}} \gg R_{\mathrm{a}}$. These reluctances are defined by

$$R_{\mathrm{a}} = \frac{l_{\mathrm{a}}}{\mu_0 \mu_{\mathrm{r,a}} A_{\mathrm{a}}} \tag{3}$$

$$R_{\mathrm{m}} = \frac{l_{\mathrm{m}}}{\mu_0 \mu_{\mathrm{r,m}} A_{\mathrm{m}}} \tag{4}$$

where l_{a}, $\mu_{\mathrm{r,a}}$, and A_{a} are the magnetic path length, relative permeability. and cross section of the auxiliary core, respectively; l_{m}, $\mu_{\mathrm{r,m}}$, and A_{m} are the corresponding values of the shared magnetic path and μ_0 is the permeability of air. It should be noted that A_{m} represents the mean core cross section of the shared magnetic path since this area is not constant along l_{m}. Moreover, A_{m} is tightly linked with the dimension c_{a} of the auxiliary core, as will be shown later in this section.

Considering the definitions from Fig. 7(a) and (b), the following observations can be made:

1) The height h_{a} of the auxiliary core must be as small as possible in order to reduce the length of the auxiliary core's magnetic path l_{a} and therefore reduce the reluctance R_{a}.
2) The width a_{a} of the core cross section must be large in order to increase the auxiliary core's cross section A_a and therefore reduce reluctance R_{a}. For the same reason, the depth of the auxiliary core d_{a} must be as close as possible to the depth d of the main core.
3) The permeability $\mu_{\mathrm{r,a}}$ of the auxiliary core must be high in order to reduce the reluctance R_{a}.
4) The air gap between the auxiliary and the main core must be kept as low as possible since this air gap introduces a constant reluctance that deteriorates the sensitivity of the transducer.
5) The number of turns N_{aux} of the auxiliary core only affects the absolute value of inductance of the auxiliary core but does not affect the sensitivity to changes in the main core's permeability. Therefore, low number of turns are suggested in order to reduce the induced voltage in the auxiliary core winding due to the flux in the main core, as will be shown in the next section.

The dimension c_{a} of the auxiliary core has a large impact on the transducer's sensitivity. For example, a small c_{a} would result in a short magnetic path l_{m}, and therefore, the auxiliary core's inductance would be mainly defined by the auxiliary core's reluctance R_{a}. On the other hand, a large c_{a} results in a large cross section A_{m} of the shared magnetic path and therefore in a small shared reluctance R_{m}, thus deteriorating the sensitivity of the transducer. For this reason, the influence of this dimension on the transducer sensitivity was studied by means of FEM simulations. In order to generalize the analysis, a per-unit system is used whereby the width w of the main core is taken as base dimension, while the relative permeability (in nonsaturated state) $\mu_{\mathrm{r,m}}$ of the main core is chosen as base permeability value.

As mentioned earlier, the goal is to find the geometry of the auxiliary core which results in the highest sensitivity of the auxiliary core's inductance L_{aux} to changes in the shared magnetic path's reluctance R_m. Therefore, the simulation consists of measuring the difference in the auxiliary core's inductance ΔL_{aux} when the permeability $\mu_{\mathrm{r,m}}$ of the main core drops by 50% for different values of c_a. Additionally, the effect of the auxiliary core's permeability $\mu_{\mathrm{r,a}}$ as well as the dimension a_a in this inductance variation is analyzed since these two parameters were found to have the greatest influence in the transducer's sensitivity.

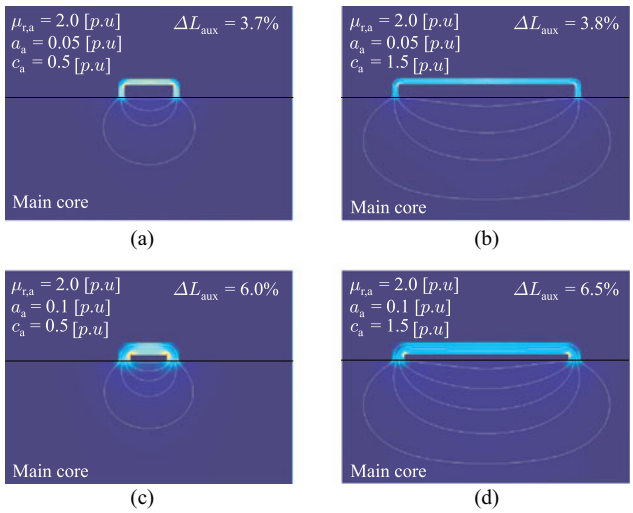

Fig. 8. Simulation examples for different auxiliary core geometries. The sensitivities, i.e., the changes ΔL_{aux} in auxiliary inductance value resulting for various values of c_a and a_a (cf., Fig. 7) are presented.

Fig. 8 shows the magnetic flux density for four exemplary simulations, whereby also the respective simulation parameters and resulting inductance variations ΔL_{aux} are shown. In Fig. 8(a), a comparatively small value of c_a was employed, resulting in a short shared magnetic path l_m. On the other hand, Fig. 8(b) shows the resulting flux density distribution for a larger value of c_a. When compared to Fig. 8(a), the flux lines in this figure show that a larger cross section A_m is achieved with this value of c_a; thus, no considerable gain in sensitivity is achieved (change in ΔL_{aux} from 3.7% to 3.8%) in spite of the larger auxiliary core length c_a. Similar effects can be seen when comparing Fig. 8(c) and (d), where a larger auxiliary core width a_a was used.

In Fig. 8(c) and (d), the results for the same variation in c_a but with a larger value of a_a are shown. This increased value of a_a results in a larger auxiliary inductance variation when compared to Fig. 8(a) and (b) due to the larger auxiliary core cross section A_a, i.e., lower auxiliary core reluctance R_a while the shared magnetic path's cross section A_m is not significantly increased, as can be seen from the flux lines in the respective figures.

The performed parametric sweeps are summarized in Fig. 9. In Fig. 9(a), the effect of different auxiliary core widths a_a for a given auxiliary core permeability ($\mu_{\mathrm{r,a}} = 2.0$) is presented. As expected, the variation ΔL_{aux} in auxiliary inductance increases with increasing a_a, as the auxiliary core cross section is also increased. Moreover, for each value of a_a, the value of c_a that maximizes the variation in auxiliary inductance can be found, as shown by the dashed line in Fig. 9(a). However, this optimum is

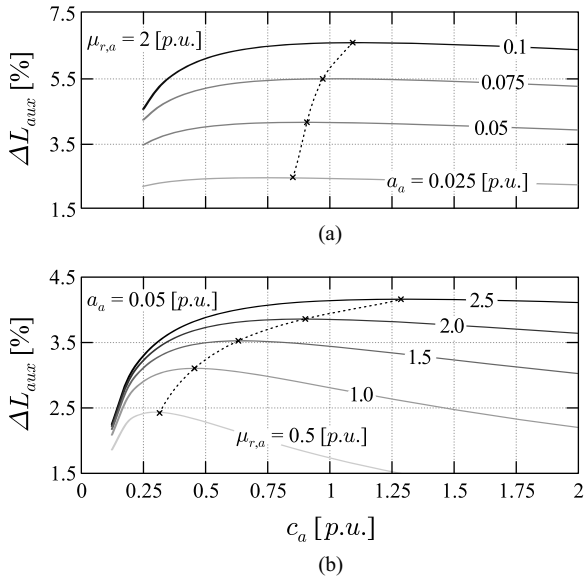

Fig. 9. Sensitivity of auxiliary core's inductance variation to different dimensions and permeability as determined by FEM simulations; (a) Constant auxiliary core permeability $\mu_{\mathrm{r,a}} = 2.0$, variable width a_a, and length c_a. (b) Constant auxiliary core width $a_a = 0.05$, variable auxiliary core permeability $\mu_{\mathrm{r,a}}$, and length c_a.

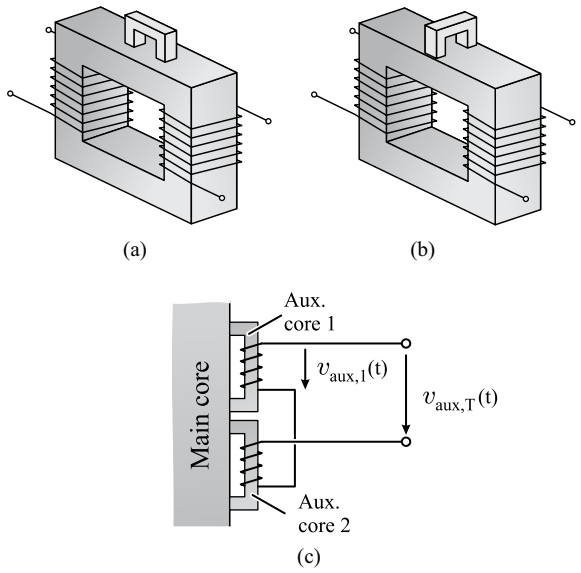

Fig. 10. Arrangement of auxiliary cores utilized to reduce the effect of the main core's flux on the auxiliary core inductance measurement. The auxiliary core can be placed so that its flux is (a) parallel or (b) orthogonal to the main flux. The auxiliary core is not shown to scale.

not highly dependent on the core length c_a, i.e., this dimension and the core width a_a can be independently selected. As a result, independent of the core length c_a, the core width a_a must always be made as large as possible.

The sensitivity of the transducer to variations in the permeability $\mu_{\mathrm{r,a}}$ of the auxiliary core is studied in Fig. 9(b) for different values of auxiliary core width c_a. As mentioned earlier, a higher permeability of the auxiliary core affects positively the sensitivity of the transducer whereby, the value of c_a which maximizes the sensitivity can be found for each value of auxiliary core relative permeability, as shown by the dashed line in Fig. 9(b). In this case, however, the optimum value of core length c_a is considerably dependent on the value of relative permeability of the auxiliary core $\mu_{\mathrm{r,a}}$. For example, if the main core and the auxiliary core possess the same permeability, i.e., $\mu_{\mathrm{r,a}} = 1.0$, the peak of sensitivity is encountered when the length of the auxiliary core c_a is 0.45 times the width w of the main core, whereas if the auxiliary core's permeability is 2.5 times that of the main core, the maximum sensitivity is found with an auxiliary core whose length c_a is 1.3 times the width w of the main core.

The previous analyses shows that, in order to achieve the highest sensitivity in the transducer, first, the relative permeability $\mu_{\mathrm{r,a}}$ of the auxiliary core must be selected as high as possible. Once this property is selected, the length c_a of the auxiliary core that maximizes the sensitivity for a given main core width w can be determined with help of Fig. 9(b).

With the rules for the selection of the auxiliary core dimensions defined, the next step in the implementation of the transducer is the proper placement of the auxiliary core, which ultimately defines the coupling of the main core's flux with the auxiliary core's winding. This topic is addressed in the following.

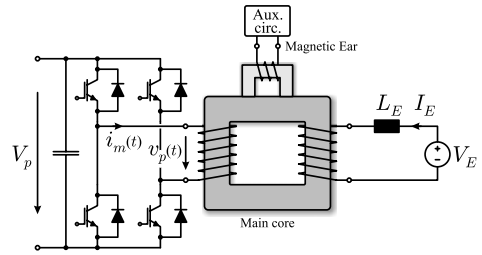

Fig. 11. Test circuit consists of a full bridge driving the transformer's main core, the magnetic flux density transducer, and an external circuit utilized to force a dc-flux component in the main core.

B. Auxiliary Core Placement

The auxiliary core offers a parallel magnetic path for the flux in the main core, and therefore, an induced voltage in the auxiliary core's winding due to the main flux is encountered. In a first step, the auxiliary core can be placed so that its magnetic flux is orthogonal to the main flux [cf., Fig. 10(b)] as opposed parallel to the main flux [cf., Fig. 10(a)] in order to reduce the coupling between the transformer's main windings and auxiliary core's winding. In order to further improve the decoupling from the main core's flux, the arrangement presented in Fig. 10(c) is considered. Here, two identical auxiliary cores with windings in opposed orientation are utilized. Nearly identical voltages are induced in the windings of these cores, but due to the opposed orientation, these induced voltages virtually cancel each other out.

In order to verify the effectiveness of this compensation scheme, consider the test circuit presented in Fig. 11, which is utilized to magnetize the core to nominal flux, while the magnetizing current i_m can be directly measured at the transformer winding. The right-hand side circuit is utilized later to force a

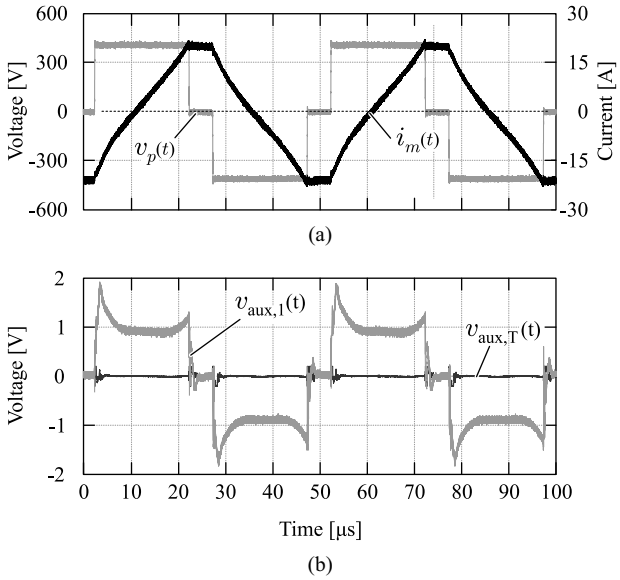

Fig. 12. Testing of the compensation arrangement shown in Fig. 10: (a) Applied voltage and resulting magnetizing current in transformer of Fig. 1. (b) Induced voltage with and without compensation arrangement.

dc-flux component in the core and can be omitted for the testing of the proposed compensation arrangement.

Fig. 12 shows the results of the compensation arrangement testing. The full bridge in Fig. 11 is supplied with $V_p = 400$ V, operated with a 20-kHz switching frequency, and 40% duty cycle was used to magnetize the transformer in Fig. 1. The resulting primary winding voltage $v_p(t)$ is shown in Fig. 12(a) together with the corresponding magnetizing current $i_m(t)$. The auxiliary cores were arranged as presented in Fig. 10, whereby the voltage $v_{\mathrm{aux,T}}(t)$ induced in the winding of the auxiliary core 1 $v_{\mathrm{aux},1}(t)$ and the compensated signal are depicted in Fig. 12(b). As can be seen, the voltage in a single auxiliary core winding is considerable and would result in a distorted measurement of the auxiliary core's inductance. When compensated, the signal $v_{\mathrm{aux,T}}(t)$ features negligible induced voltage, thus, this arrangement can be reliably used in order to extract the auxiliary core's inductance. This last task is performed by the driving circuit of the auxiliary core, as described in the next section.

It should be noted that the proposed magnetic flux density transducer can be implemented on virtually any core shape, given its noninvasive characteristic which does not require specially shaped cores in order to be implemented.

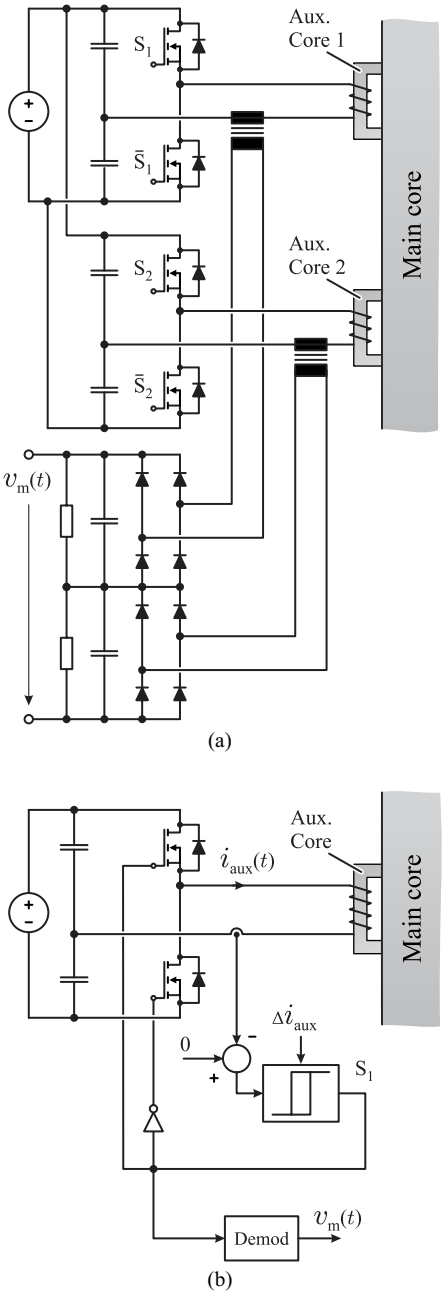

Fig. 13. Driver circuits utilized to extract the inductance value of the auxiliary core. (a) Interleaved bridges operated at a constant frequency and with minimum filtering requirements. (b) Constant peak-peak, variable frequency-controlled driver. The inductance value is translated into the operating frequency of the bridge.

C. Drive Circuit

In order to extract the inductance value from the auxiliary core, a constant amplitude high-frequency excitation voltage is used in order to drive the auxiliary core, whereby the peak value of the current through the inductor is inversely proportional to its inductance value. This current is later rectified and filtered, generating a low-frequency signal directly related to the value of the auxiliary core's inductance and therefore to the magnetization state of the main core.

With the aforementioned driving circuit concept, however, the filtering stage at the output of the driving circuit defines the bandwidth of the transducer, thus, in order to improve this bandwidth limitation, the driving circuit of Fig. 13(a) is proposed. This circuit consists of two interleaved half-bridges phase-shifted by 90 ° driving each auxiliary core (each of these cores is then replaced by another pair of cores to compensate for the induced voltage, as shown in Fig. 10) with a switching frequency several times higher than the main core's excitation frequency. Each bridge forces a current through their corresponding

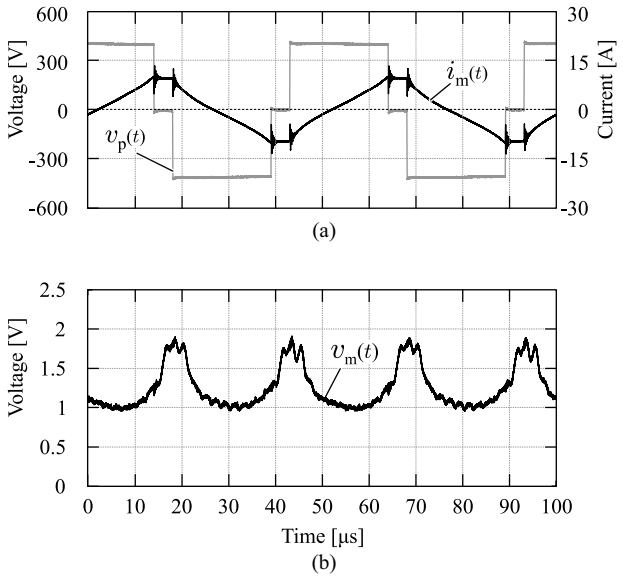

Fig. 14. Performance of the magnetic flux density transducer for unbiased operation. (a) Excitation voltage $v_p(t)$ applied by the test circuit and the resulting magnetizing current $i_m(t)$. (b) Output signal of the magnetic flux density transducer $v_m(t)$.

auxiliary cores. Respective current transformers are used to sense this current which, is then rectified by diode bridges. The output diode rectifiers are connected in series, causing the phase shifted currents to compensate the ripple in the output signal $v_m(t)$, reducing the amount of required output filter capacitance and therefore increasing the bandwidth of the transducer.

An alternative drive circuit is shown in Fig. 13(b). The main idea of this circuit is to operate the bridge at a constant peak-to-peak current by controlling the current with a hysteresis controller whereby the switching frequency of the bridge is inversely proportional to the inductance of the auxiliary core. The switching signal at the output of the controller can be later demodulated into an analog signal containing the information about the magnetization state of the main core.

The final transducer comprising two pairs of auxiliary cores based on EPCOS EQ30/8 cores and the described drive circuit was built and is shown in Fig. 15. This arrangement of cores [one pair for each auxiliary core in Fig. 13(a)] driven by the circuit presented in Fig. 13(a) was tested with the setup shown in Fig. 11. The resulting output signal $v_m(t)$ of the transducer is presented in Fig. 14(b). As shown in this figure, the transducer outputs a high signal value when the magnetizing current $i_m(t)$ reaches a high value, i.e., when the flux in the main core is entering saturation region. On the other hand, the output signal $v_m(t)$ stays low during the zero crossing of the magnetizing current, i.e., when the magnetic flux in the main core is zero. The slight phase-shift between the peak magnetizing current $i_m(t)$ and the transducer's output signal $v_m(t)$ is due to the output filter capacitor of the drive circuit. However, since this signal is sampled only at the end of the freewheeling period, this phase shift does not deteriorate the behavior of the closed-loop controller, as described in Section V of this paper.

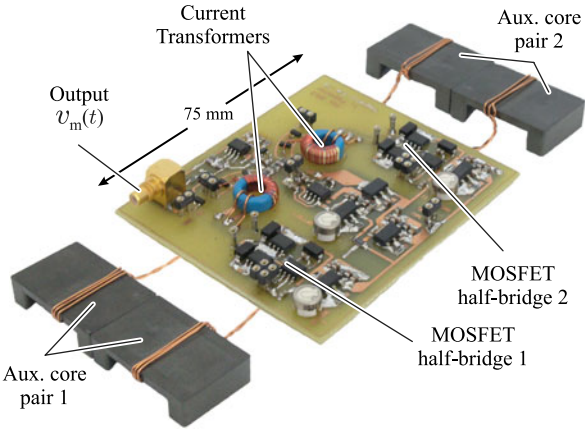

Fig. 15. Hardware realization of The Magnetic Ear flux density transducer.

The aforementioned behavior of the magnetic flux density transducer, comprising the drive circuit from Fig. 13(a), demonstrates the utility of this measurement concept, as the output signal of the transducer is directly related to the magnetization state of the main core. It is now the task of the digital controller to sample the transducer output signal $v_m(t)$ in order to detect and finally actively correct a biased magnetization state of the main core.

D. Sampling Methods

The output signal shown in Fig. 14(b) continuously changes as the magnetization state of the main core is varying. This signal can be sampled at a high sampling rate, e.g., ten times higher than the frequency of the main core excitation. A lookup table implemented in the digital control platform is utilized in order to translate the signal $v_m(t)$ into the instantaneous value of the magnetic flux density in the main core.

For the purpose of operating the main core with unbiased flux density, however, sampling The Magnetic Ear's output signal during the freewheeling states of the full-bridge (coinciding with the moment when the flux density is the highest in the main core) would suffice to obtain the dc magnetization state of the main core. This behavior can be seen from Fig. 17, where a dc component $\bar{I}_m$ in the magnetizing current, i.e., in the main core's flux density was induced by adjusting the duty cycles on the test bridge [cf., Fig. 17(a)]. Fig. 17(b) shows the resulting output signal $v_m(t)$ from the flux density transducer whereby a clear difference in its peak value can be noticed during two consecutive freewheeling intervals. Due to the biased flux density operation, the output signal $v_m(t)$ features its peak value at the end of the positive semicycle since it is at this point when the main core's permeability is at its minimum, i.e. the auxiliary core's inductance is at its minimum.

The difference between the peak values of the output signal at the end of the positive and negative semicycles is directly related to the biased magnetization state of the main core. This means that keeping this difference at its minimum is equivalent to minimizing the dc component of main core's magnetic flux density. This strategy is used in order to actively control the dc

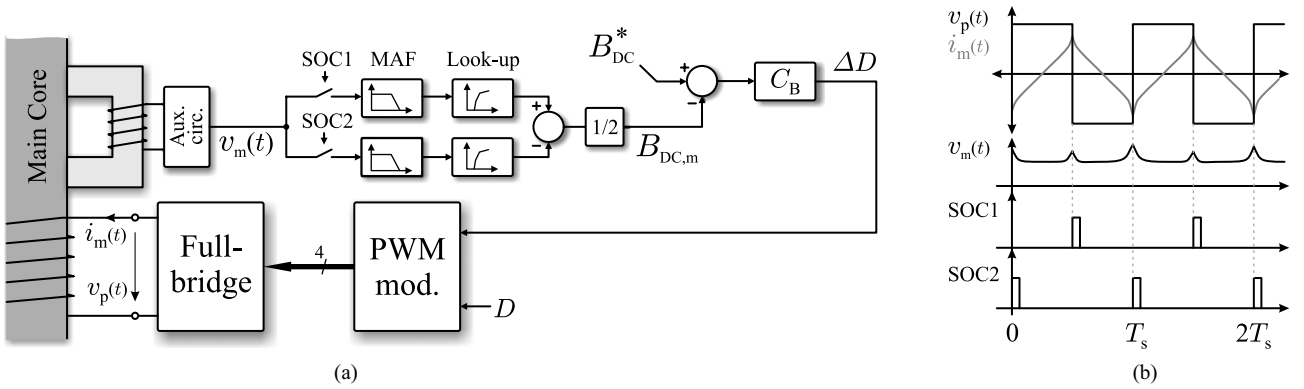

Fig. 16. (a) Feedback/balancing scheme: the output of The Magnetic Ear, $v_m\,(t)$ is sampled by the ADC in the DSP board. By sampling on each switching event of the full-bridge [part (b)], a construction of the dc-flux density in the core is obtained and used to balance the flux in the main core.

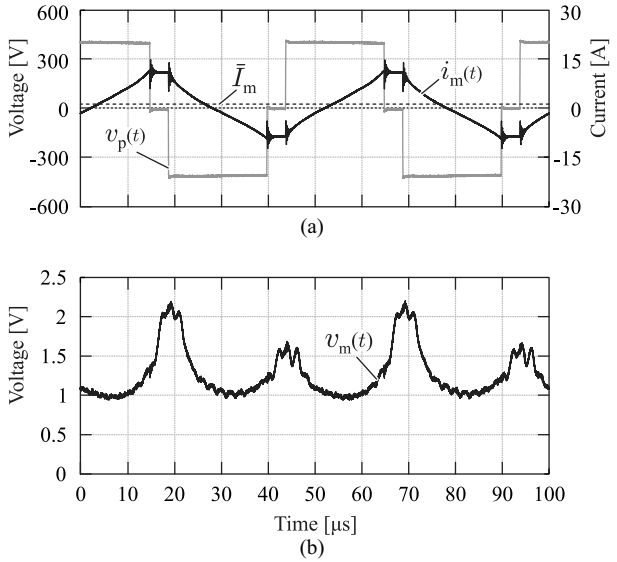

Fig. 17. Performance of the magnetic flux density transducer for biased main core operation. (a) Excitation voltage $v_p\,(t)$ applied by the test circuit and the resulting magnetizing current $i_m\,(t)$ with dc component $\bar{I}_m$ in the magnetizing current. (b) Output signal of the magnetic flux density transducer $v_m\,(t)$.

component of the magnetic flux density in the core, as will be experimentally shown in the next section.

IV. Closed-Loop Operation

The output $v_m\,(t)$ of The Magnetic Ear must be fed into the DSP controller of the full-bridge converter in order to actively compensate the dc bias. In order to obtain the value of $B_{\rm dc}$ in the main core, the scheme shown in Fig. 16(a) was used. As can be seen from Fig. 16(b), different start of conversion (SOC) signals (the signals that trigger a conversion of the analog-to-digital converter of the DSP), i.e., SOC1 and SOC2 are generated in the positive and negative edges of the full-bridge output voltage $v_p(t)$. The sampled values at each of these instants are independently stored and filtered by moving average filters (MAF). In order to obtain the final flux density value, a look-up table is built based on the measurements of The Magnetic Ear output and the magnetic flux density calculated from the voltage applied to the core. It should be noted that the gain from The Magnetic Ear output to flux density is highly nonlinear since, when the core is close to saturation, a small increase in the flux density generates a large change in the output signal of the transducer whereas, when the core is in linear region, the change in the output signal with respect to changes in the flux density is several times smaller.

The outputs of the look-up tables are the absolute values of flux density in the main core at the switching instants. Therefore, the subtraction of these two signals gives twice the value of dc flux density component $B_{\rm dc}$ inside core. For example, in the steady-state operation, if no dc bias is present in the core, the output of The Magnetic Ear would be identical at the positive and negative edges of the applied voltage $v_p\,(t)$. As a consequence, the output of the look-up tables, the flux density at the switching times, would be identical and, thus, the measured dc flux density component would be zero.

In order to control the dc flux density in the core, a standard PI controller, C_B is used [cf., Fig. 16(a)]. The output of this controller is the additional duty cycle ΔD required to increase or decrease the dc voltage applied to the primary winding. In the PWM modulator, this signal is combined with the duty cycle D calculated to transfer desired amount of power, which was left to 40% in this case.

Several experiments in different testing conditions were realized in order to study the dynamic performance of this feedback loop. The first test, shown in Fig. 18(a), consists of a step response from -30 to 30 mT in the dc flux density component reference $B_{\rm dc}*$. As can be seen, the feedback loop is successfully able to regulate within 5 ms the dc component $B_{\rm dc}$ in the magnetic flux density. Considering the slow dynamics of the potential sources for dc components in the voltage applied to the transformer (e.g., differences in switching times, forward voltage drops, and gate driving signal delays), this response time is considered appropriate. Fast modifications in loading conditions can also cause imbalances in the dc flux density component, as described in [16]. However, with modern digital control platforms, this problem can be solved by introducing a middle step in the duty-cycle actualization, as described in [20]. Additionally in Fig. 18(b) and (c), the voltage and current through the transformer together with the transducer's output signal are

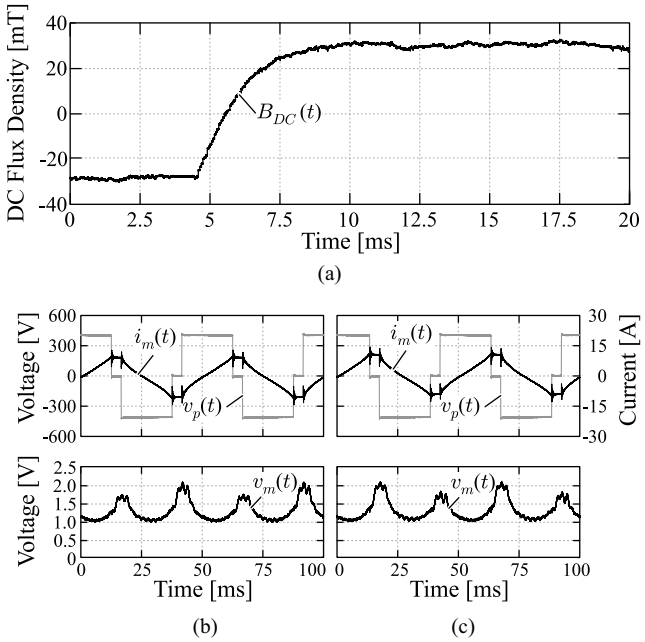

Fig. 18. Step response of the feedback loop comprising the proposed transducer is shown in (a). The voltage $v_p\,(t)$ and current $i_m\,(t)$ on the transformer and magnetic ear output $v_m\,(t)$ (b) before and (c) after the dc flux-density step.

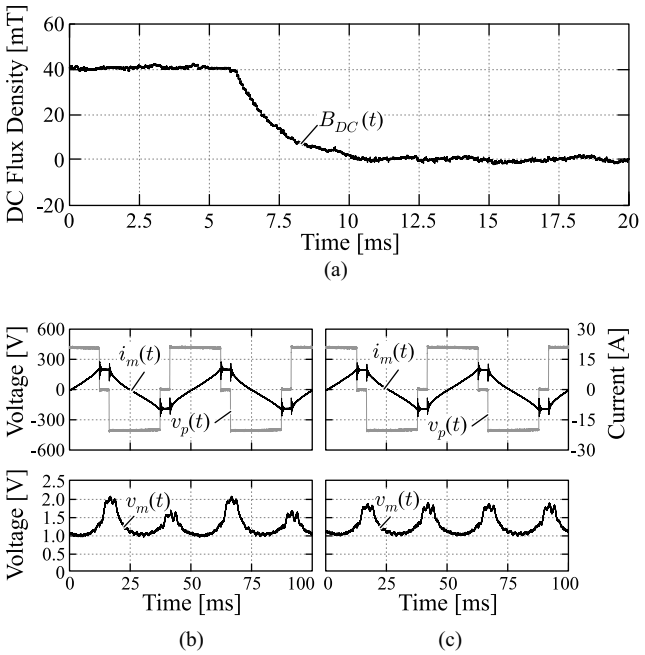

Fig. 19. Response of the feedback loop to external disturbance utilizing the proposed transducer. The voltage $v_p\,(t)$ and current $i_m\,(t)$ on the transformer and magnetic ear output $v_m\,(t)$ (b) before and (c) after the activation of the compensation loop.

presented before and after the application of the reference step in $B_{\rm dc}*$. Here, the relation between the output signal $v_m\,(t)$ and the transformer's flux density can be clearly seen as this output signal exhibits higher values at the positive voltage slopes before the step, meaning negative dc bias on the flux density. On the other hand, after the step in flux-density, the higher values in the output signal are seen at the negative voltage slopes, which shows that the dc flux density component has changed to a negative value.

The second performed test consists of forcing an external dc flux density component with the external dc source and inductor shown in Fig. 11. By adjusting the current I_E, the dc flux density component $B_{\rm dc,E}$ in the main core can be adjusted. This dc component is measured with The Magnetic Ear flux density transducer and used in the feedback loop in order to compensate for it with the main full bridge. The result of this test is shown in Fig. 19(a). Here, the feedback loop is left off until $t =$ 6 ms, whereby before this time a forced dc component $B_{\rm dc,E} =$ 40 mT can be noticed. As the dc flux density component feedback loop is activated at $t = 6$ ms, the dc flux density component $B_{\rm dc}$ is regulated to zero after 5 ms, achieving an unbiased flux density operation. The output of the transducer before and after the activation of the feedback loop is shown in Figs. 11(b) and (c), respectively. As can be seen, the transducer output features an unsymmetrical behavior before the compensation loop is activated, which implies a biased operation of the flux density. As the compensation loop is activated, the dc flux density component is controlled to zero, which can be seen from the symmetrical behavior of the transducer's output signal.

An additional test consists of ramping on the duty-cycle while controlling the dc flux density component to zero was performed. The duty-cycle variation and the respective dc flux density component value $B_D C(t)$ are presented in Fig. 20(a). The duty cycle ramp starts at 25% and reaches 45%. The dc flux density component stays well regulated during the duty-cycle ramp, with variations below ± 1 mT. Moreover, the voltage and current in the transformer for 25% duty cycle and 45% duty cycle are presented in Figs. 20(b) and (c), respectively, where the change in the voltage's duty-cycle can be clearly seen. Additionally, the output signal of The magnetic ear is affected for lower duty-cycles as expected, reaching low values due to the lower reached magnetization state of the core.

Very often dc–dc converters are coupled with single-phase power-factor-correction rectifiers, which inherently generate a double frequency component in the dc-link's voltage. In order to test the performance of the compensation loop under these conditions, a 100-Hz voltage component was inserted in the driving bridge's dc-link voltage, as shown in Fig. 21(b). The response of the feedback loop presented in Fig. 21(a) shows that the dc flux density component $B_{\rm dc}(t)$ is kept regulated under this variation in the dc-link voltage and during the ramping of the converter's duty cycle.

These tests show the effectiveness of the proposed magnetic flux density transducer and its respective drive circuit and feedback scheme, ensuring the unbiased dc flux density operation of the transformer.

V. Conclusion

Medium-frequency transformers are critical components within high-power dc–dc converters. In order to maintain a high reliability of the system, the operation of these transformers

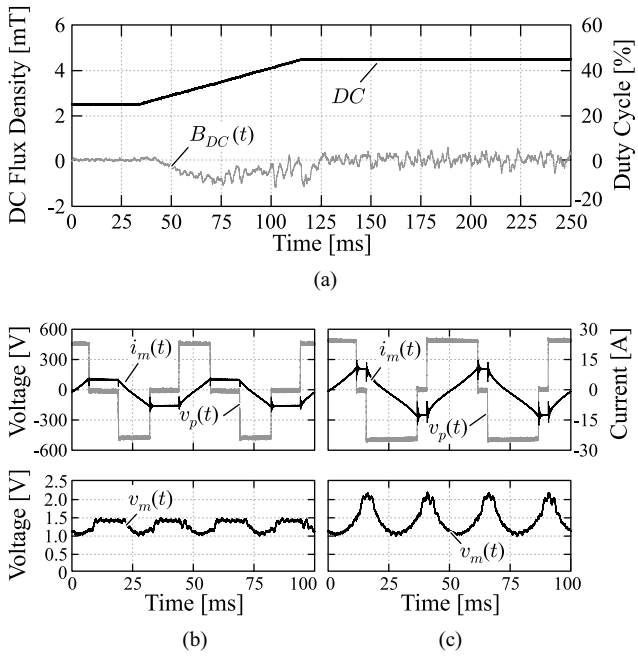

Fig. 20. Feedback loop response to change in the duty-cycle, representing a variation in transferred power. In (a), the change in the duty cycle and the respective response of the dc-flux density component $B_{\rm dc}(t)$ are shown. In (b) and (c), the transformer voltage $v_p(t)$ and current $i_m(t)$ together with the transducer's output $v_m(t)$ are shown at low duty-cycle and higher duty-cycle values, respectively.

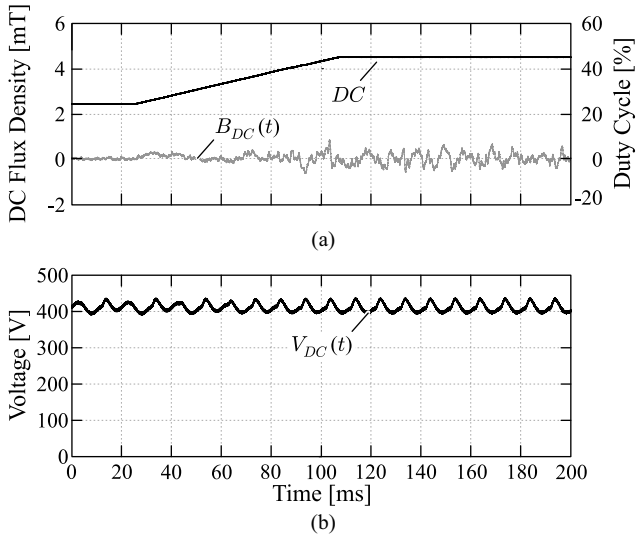

Fig. 21. Response of the feedback loop to variation in the duty-cycle and a 100-Hz harmonic in the dc-link voltage. In (a), the duty cycle value and the controlled flux-density are presented $B_{\rm dc}(t)$, while (b) shows the dc-link voltage with the mentioned 100 Hz.

under unbiased flux density must be ensured. Therefore, a thorough revision of the previously proposed and analyzed flux balancing concepts was realized, highlighting the need for a new concept which complies with the requirements of medium-frequency transformers. As a result, a new concept for a flux density transducer "The Magnetic Ear" was proposed. This magnetic flux density transducer was successfully implemented on a real 166-kW/20-kHz transformer, ensuring unbiased dc flux density operation of the transformer. In order to implement this transducer, first, a general analysis of the tradeoffs in the selection the of the auxiliary core geometry was performed, leading to clear rules which can be utilized to appropriately select the dimensions that best suit the main transformer dimensions. The drive circuit utilized to extract the inductance value of the auxiliary core and therefore to extract the information about the magnetization state of the core was presented. Here, a drive circuit with large bandwidth was utilized, enabling the implementation of a fast feedback loop, which was ultimately utilized to actively control the dc magnetization state of the core, as demonstrated experimentally under a variety of operating conditions.

REFERENCES

[1] K. O'Meara, "Passive balancing of transformer flux in power converters," in *Proc. 10th Nat. Solid-State Power Convers. Conf.*, Mar. 1983, vol. A1, pp. 1–11.

[2] G. Ortiz, J. Biela, D. Bortis, and K. J. W. , "1 Megawatt, 20 kHz, isolated, bidirectional 12 kV to 1.2 kV DC-DC converter for renewable energy applications," in *Proc. Int. Power Electron. Conf.*, Jun. 2010, pp. 3212–3219.

[3] G. Ortiz, M. Leibl, J. Kolar, and O. Apeldoorn, "Medium frequency transformers for solid-state-transformer applications—Design and experimental verification," in *Proc. Power Electron. Drive Syst.*, 2013, pp. 1285–1290.

[4] J. Muhlethaler, J. Biela, J. Kolar, and A. Ecklebe, "Core losses under DC bias condition based on Steinmetz parameters," in *Proc. Power Electron. Conf.*, 2010, pp. 2430–2437.

[5] R. Patel, "Detecting impending core saturation in switched-mode power converters," in *Proc. 7th Nat. Solid-State Power Convers. Conf.*, Mar. 1980, vol. B3, pp. 1–11.

[6] S. Klopper and J. A. Ferreira, "A sensor for balancing flux in converters with a high-frequency transformer link," *IEEE Trans. Ind. Appl.*, vol. 33, no. 3, pp. 774–779, May/Jun. 1997.

[7] D. Wilson, "A new pulsewidth modulation method inherently maintains output transformer flux balance," in *Proc. 8th Nat. Solid-State Power Convers. Conf.*, Apr. 1981, vol. D1, pp. 1–14.

[8] F. Stögerer, J. W. Kolar and U. Drofenik, "A novel concept for transformer volt second balancing of VIENNA rectifier III based on direct magnetizing current measurement," in *Proc. Nordic Workshop Power Ind. Electron. Workshop*, Jun. 2000, pp. 134–139.

[9] W. M. Polivka, A. Cocconi, and S. Cuk, "Detection of magnetic saturation in switching converters," in *Proc. Power Convers. Int. Conf.*, Mar. 1982, pp. 584–597.

[10] A. Gerstman and S. Ben-Yaakov, "Zeroing transformer's DC current in resonant converters with no series capacitors," in *Proc. Energy Convers. Congr. Expo.*, Sep. 2010, pp. 4028–4034.

[11] L. Daniel, C. R. Sullivan, and S. R. Sanders, "Design of microfabricated inductors," *IEEE Trans. Power Electron.*, vol. 14, no. 4, pp. 709–723, Jul. 1999.

[12] R. Kuttner, "Circuit techniques for eliminating primary current unbalance in push-pull power converters," in *Proc. 7th Nat. Solid-State Power Convers. Conf.*, Mar. 1980, vol. F2, pp. 1–9.

[13] F. P. Dawson, "DC-DC converter interphase transformer design considerations: Volt-seconds balancing," *IEEE Trans. Magn.*, vol. 26, no. 5, pp. 2250–2252, Sep. 1990.

[14] P. Ripka, "Review of fluxgate sensors," *Sens. Actuat. A: Phys.*, vol. 33, no. 3, pp. 129–141, 1992.

[15] H. T. Paul Mettler. (1987). "Saturation monitoring arrangement and method of control for a frequency-converter welding device," Patent US 4 709 132 A, 11 24, [Online]. Available: http://www.google.com/patents/US4709132

[16] R. Redl, N. Sokal, and C. W. Schaefer, "Transformer saturation and unusual system oscillations in capacitively coupled half-bridge or full-bridge forward converters: Causes, analyses, and cures," in *Proc. Power Electron. Spec. Conf.*, Apr. 1988, pp. 820–828.

[17] O. Garcia, P. Zumel, A. De Castro, P. Alou, and J. Cobos, "Current self-balance mechanism in multiphase buck converter," *IEEE Trans. Power Electron.*, vol. 24, no. 6, pp. 1600–1606, Jun. 2009.

[18] D. Costinett, D. Seltzer, D. Maksimovic, and R. Zane, "Inherent volt-second balancing of magnetic devices in zero-voltage switched power converters," in *Proc. Appl. Power Electron. Conf. Expo.*, 2013, pp. 9–15.
[19] S. Han, I. Munuswamy, and D. Divan, "Preventing transformer saturation in bi-directional dual active bridge buck-boost DC-DC converters," in *Proc. Energy Convers. Congr. Expo.*, Sep. 2010, pp. 1450–1451.
[20] J. Claassens and I. Hofsajer, "A flux balancer for phase shift ZVS DC-DC converters under transient conditions," in *Proc. Appl. Power Electron. Conf. Expo.*, Mar. 2006, pp. 523–527.

Gabriel Ortiz (M'10) studied electronics engineering at Universidad Técnica Federico Santa María, Valparaíso, Chile, joining the power electronics group early on 2007. He received the M.Sc. degree in December 2008, and he has been working toward the Ph.D. degree at the Power Electronic Systems Laboratory, ETH Zurich, Zurich, Switzerland, since February 2009.

During his Master's thesis, he worked with reconfiguration of regenerative and nonregenerative cascaded multilevel converters under fault condition, obtaining maximum qualification in his thesis examination. The focus of his research is in solid state transformers for future smart grid implementations and traction solutions. Specifically, his PhD. research deals with the modeling, optimization, and design of high-power dc–dc converters operated in the medium frequency range with focus on modeling of soft-switching processes in IGBTs and medium-frequency transformer design, among others.

Lukas Fässler was born in Wetzikon, Switzerland, on April 18, 1986. He studied electrical engineering with a focus on power electronics, drive systems, and high voltage technology at the Swiss Federal Institute of Technology (ETH), Zurich, Switzerland, where he received the M.Sc. degree in Summer 2011.

After working on an ultrahigh speed spinning ball project during an internship with the company Levitronix, he designed and constructed a 166-kW/20-kHz NPC module as his Master's thesis at the Power Electronic Systems Laboratory, ETH Zurich, which was a part of the 1-MW Megacube solid-state transformer project. Since 2012, he has been working for the ETH spin-off company Enertronics.

Johann Walter Kolar (S'94–M'91–SM'04–F'10) received the M.Sc. and Ph.D. degree (*summa cum laude/promotio sub auspiciis praesidentis rei publicae*) from the University of Technology Vienna, Vienna, Austria.

Since 1984, he has been working as an independent international consultant in close collaboration with the University of Technology Vienna, in the fields of power electronics, industrial electronics, and high performance drives. He has proposed numerous novel converter topologies and modulation/control concepts, e.g., the VIENNA Rectifier, the Swiss Rectifier, and the three-phase ac–ac Sparse Matrix Converter. He has published more than 450 scientific papers in international journals and conference proceedings, and has filed more than 85 patents. He was appointed a Professor and the Head of the Power Electronic Systems Laboratory at the Swiss Federal Institute of Technology (ETH) Zurich, Zurich, on Feb. 1, 2001. The focus of his current research is on ac–ac and ac–dc converter topologies with low effects on the mains, e.g., for data centers, more-electric-aircraft, and distributed renewable energy systems, and on solid-state transformers for smart microgrid systems. Further main research areas are the realization of ultracompact and ultraefficient converter modules employing latest power semiconductor technology (SiC and GaN), micropower electronics and/or power supplies on chip, multidomain/scale modeling/simulation and multiobjective optimization, physical model-based lifetime prediction, pulsed power, and ultrahigh speed and bearingless motors. He initiated and/or is the founder/cofounder of four spin-off companies targeting ultrahigh speed drives, multidomain/level simulation, ultracompact/efficient converter systems, and pulsed power/electronic energy processing. In 2006, the European Power Supplies Manufacturers Association awarded the Power Electronics Systems Laboratory of ETH Zurich as the leading academic research institution in Power Electronics in Europe.

Dr. Kolar has been appointed as an IEEE Distinguished Lecturer by the IEEE Power Electronics Society in 2011. He received the Best Transactions Paper Award of the IEEE Industrial Electronics Society in 2005, the Best Paper Award of the ICPE in 2007, the 1st Prize Paper Award of the IEEE IAS IPCC in 2008, the IEEE IECON Best Paper Award of the IES PETC in 2009, the IEEE PELS Transaction Prize Paper Award 2009, the Best Paper Award of the IEEE/ASME TRANSACTIONS ON MECHATRONICS 2010, the IEEE PELS Transactions Prize Paper Award 2010, the Best Paper 1st Prize Award at the IEEE ECCE Asia 2011, and the 1st Place IEEE IAS Society Prize Paper Award 2011 and the IEEE IAS EMC Paper Award 2012. Furthermore, he received the ETH Zurich Golden Owl Award 2011 for Excellence in Teaching. He also received an Erskine Fellowship from the University of Canterbury, New Zealand, in 2003. He is a Member of the International Steering Committees and Technical Program Committees of numerous international conferences in the field (e.g., Director of the Power Quality Branch of the International Conference on Power Conversion and Intelligent Motion). He is the founding Chairman of the IEEE PELS Austria and Switzerland Chapter and Chairman of the Education Chapter of the EPE Association. From 1997 through 2000, he has been serving as an Associate Editor of the IEEE TRANSACTIONS ON INDUSTRIAL ELECTRONICS and since 2001, as an Associate Editor of the IEEE TRANSACTIONS ON POWER ELECTRONICS. Since 2002, he has also been an Associate Editor of the *Journal of Power Electronics of the Korean Institute of Power Electronics*, and a member of the Editorial Advisory Board of the IEEE TRANSACTIONS ON ELECTRICAL AND ELECTRONIC ENGINEERING.

Oscar Apeldoorn received the M.Sc. and Ph.D. degrees from the Technical University Aachen, Aachen, Germany, in 1991 and 1997, respectively.

He then worked at ABB Power Electronic and MVD, Turgi, Switzerland. Until 1999, he was responsible for the development of new high-power converters. Following this, he joined the power electronics innovation and in this responsibility he developed new converter concepts and power semiconductors. From 2001 to 2005, he was Incharge of the power electronics development team. In parallel to his following study for Executive Master of Business Administration at the University of St. Gallen Switzerland, he was responsible for the development of new high power IGCTs applications and converters. After his graduation in 2007, he became Local Technology Manager in the business unit for power electronics and medium voltage drives.